

PGMAN: An Unsupervised Generative Multi-adversarial Network for Pan-sharpening

Huanyu Zhou, Qingjie Liu, *Member, IEEE*, Yunhong Wang, *Fellow, IEEE*

Abstract—Pan-sharpening aims at fusing a low-resolution (LR) multi-spectral (MS) image and a high-resolution (HR) panchromatic (PAN) image acquired by a satellite to generate an HR MS image. Many deep learning based methods have been developed in the past few years. However, since there are no intended HR MS images as references for learning, almost all of the existing methods down-sample the MS and PAN images and regard the original MS images as targets to form a supervised setting for training. These methods may perform well on the down-scaled images, however, they generalize poorly to the full-resolution images. To conquer this problem, we design an unsupervised framework that is able to learn directly from the full-resolution images without any preprocessing. The model is built based on a novel generative multi-adversarial network. We use a two-stream generator to extract the modality-specific features from the PAN and MS images, respectively, and develop a dual-discriminator to preserve the spectral and spatial information of the inputs when performing fusion. Furthermore, a novel loss function is introduced to facilitate training under the unsupervised setting. Experiments and comparisons with other state-of-the-art methods on GaoFen-2, QuickBird and WorldView-3 images demonstrate that the proposed method can obtain much better fusion results on the full-resolution images. Code is available¹.

Index Terms—pan-sharpening, image fusion, unsupervised learning, generative adversarial network

I. INTRODUCTION

DUE to physical constraints [1], many satellites such as QuickBird, GaoFen-1, 2, WorldView I, II only offer a pair of modalities at the same time: multi-spectral (MS) images at a low spatial resolution and panchromatic (PAN) images at a high spatial resolution but a low spectral resolution. In many practical applications, it is desired to use high-resolution (HR) MS images. Pan-sharpening, which combines the strengths of an MS image with a PAN image to generate an HR MS image, provides a good solution to this.

Over the past few decades, researchers in the remote sensing community have developed various methods for pan-sharpening. These methods, to distinguish them from the recently proposed deep learning models we called them traditional pan-sharpening methods, can be mainly divided into three categories: 1) Component substitution (CS)-based methods, 2) Multi-resolution analysis (MRA)-based methods, and 3) Model-based methods. The CS methods convert MS

images into a new space, in which one component is replaced with the spatial parts of the PAN, and then perform an inverse transformation to obtain the pan-sharpened images. Intensity-hue-saturation technique (IHS-based methods [2]), principal component analysis (PCA-based methods [3], [4]), and Gram-Schmidt (GS [5] method) are those widely adopted transformations. The MRA methods apply multi-resolution algorithms to extract the spatial information of PAN images and then inject them into MS images. Some representative methods include the modulation transfer function (MTF [6], [7]), and the smoothing filter-based intensity modulation (SFIM [8]). The model-based methods attempt to build interpretable mathematical models of the input PAN and MS and the ideal HR MS. They usually need to solve an optimization problem to parameterize the models. A typical method is band-dependent spatial detail (BDSD [9]) model. These traditional methods are widely used in practice, however, their ability to solve high nonlinear mapping is limited and thus often suffer from spatial or spectral distortions.

Recently, deep learning techniques have made great successes in various computer vision tasks, from low-level image processing to high-level image understandings [10]–[12]. Convolution neural networks (CNNs) have shown a powerful ability of modeling complex non-linear mappings and the superiority of solving image-enhancing problems such as single image super-resolution [13], [14]. Inspired by this, many deep learning models have been developed for pan-sharpening. PNN [15] introduces SRCNN [16] to pan-sharpening and designs a fusion network which is also a 3-layered CNN. PanNet [17] borrows the idea of skip-connection from ResNet [18] to build deeper networks and trains the model on the high-frequency domain to learn the residual between the up-sampled LR MS image and the desired HR MS image. DRPNN [19] also learns from ResNet [18] and designs a deeper CNN with 11 layers. MSDCNN [20] tries to explore the multi-scale structures from images by using different sizes of filters and combining a shallow network and a deep network. TFNet [21] builds a two-stream fusion network and designs a variant of UNet [22] to solve the problem. PSGAN [23] improves the TFNet [21] by using generative adversarial training [24].

These deep learning methods for pan-sharpening have achieved satisfactory performances. However, they cannot be optimized without supervised images and hence are hard to obtain optimal results on the full-resolution images. To be specific, the existing works require ideal HR MS images which do not exist to train networks. To optimize the networks, they down-sample PAN and MS images and take the original MS image as targets to form training samples. In the testing

Authors are with the State Key Laboratory of Virtual Reality Technology and Systems, Beihang University and Hangzhou Innovation Institute, Beihang University. Email: {zhysora, qingjie.liu, yhwang}@buaa.edu.cn. Qingjie Liu is the corresponding author of this paper. This work was supported by NSFC Nos. 41871283 and 61601011.

¹<https://github.com/zhysora/PGMAN>

stage, evaluations are also conducted on the down-sampled images. However, for remote sensing images, this protocol may cause a gap between down-sampled images and the original ones. Different from natural images, remote sensing images are usually in deeper bit depths and with distinct pixel distributions. These supervised methods may have good performances in the down-sampled image domain, however, they generalize poorly to the original full-scale images, which makes them lack practicality.

To overcome this drawback, we propose an unsupervised generative multi-adversarial network, termed PGMAN. PGMAN focuses on unsupervised learning and is trained on the original data without down-sampling or any other pre-processing steps to make full use of original spatial and spectral information. Our method is inspired by CycleGAN [25]. We use a two-stream generator to extract modality-specific features from PAN and MS images, respectively. Since we do not have target images to calculate losses, the only way for us to verify the quality of the generated images is the consistency property between the pan-sharpened images and the PAN and MS images, *i.e.*, the degraded versions of the HR MS images, both spectral and spatial degradations, should be as close as possible to the PAN and MS images. To realize this, we build two discriminators, one is to distinguish the down-sampled fusion results from the input MS images, and the other one is to distinguish the grayed fusion images from the input PAN. Furthermore, inspired by the non-reference metric *QNR* [26], we introduce a novel loss function to boost the quality of the pan-sharpened images. Our major contributions can be summarized as follows:

- We design an unsupervised generative multi-adversarial network for pan-sharpening, termed PGMAN, which can be trained on the full-resolution PAN and MS images without any pre-processing. It takes advantage of the rich spatial and spectral information of the original data and is consistent with the real application environment.
- For the purpose of being consistent with the original PAN and MS images, we transform the fusion result back to PAN and LR MS images and design a dual-discriminator architecture to preserve the spatial and spectral information.
- Inspired by the *QNR* metric, We introduce a novel loss to optimize the network under the unsupervised learning framework without reference images.
- We conduct extensive experiments on GaoFen-2, QuickBird and WorldView-3 images to compare our proposed model with the state-of-the-art methods. Experimental results demonstrate that the proposed method can achieve the best results on the full-resolution images, which clearly show its practical value.

The remainder of this paper is organized as follows. The related works and background knowledge are introduced in Section II. The details of our proposed method are described in Section III. Section IV shows the experiments and the results. Finally, the conclusions are given in Section V.

II. RELATED WORK

Deep learning techniques have achieved great success in diverse computer vision tasks, inspiring us to design deep learning models for the pan-sharpening problem. Observing that pan-sharpening and single image super-resolution share a similar spirit and motivated by [16], Masi et al. [15] proposes a three-layered convolutional neural network (CNN) based pan-sharpening method. Following this work, increasing research efforts have been devoted to developing deep learning based pan-sharpening. For instance, Zhong et al. [27] present a CNN based hybrid pan-sharpening method. Recent studies [28], [29] have suggested that deeper networks will achieve better performance on vision tasks. The first attempt at applying the residual network is PanNet [17]. They adopt a similar idea to [30] and [31] but employ ResNet [18] to predict details of the image. In this way, both spatial and spectral information could be preserved well.

Generative adversarial networks (GANs), proposed by Goodfellow et al. [24], have achieved attractive performance in various image generation tasks. The main idea of GANs is to train a generator with a discriminator, adversarially. The generator learns to output realistic images to cheat the discriminator while the discriminator learns to distinguish the generated images from real ones. However, the difficulty of stable training of GANs remains a problem. DCGAN [32] introduces CNN to GANs and drops the pooling layer, which improves the performance. LSGAN [33] replaces the sigmoid cross entropy loss function with the least squares loss function to avoid vanishing gradients problem. WGAN [34] leverages the Wasserstein distance as the objective function and uses weight clipping to stabilize the training process. WGAN-GP [35] penalizes norms of gradients of discriminators with respect to its input rather than uses weight clipping. SAGAN [36] adds self-attention modules for long-range dependency modeling. To speed up convergence and ease the training process, we choose WGAN-GP as the basic GAN to build our model.

Recently, researchers do not limit GANs in one-generator-one-discriminator architecture and try to design multiple generators and discriminators for dealing with difficult tasks. GMAN [37] extends GANs to multiple discriminators and endows them with two roles: formidable adversaries and forgiving teachers. One is a stronger discriminator while another is weaker. CycleGAN [25] designs two pairs of generators and discriminators and proposes a cycle consistency loss to reduce the space of possible mapping functions. MsCGAN [38] is a multi-scale adversarial network consisting of two generators and two discriminators handling different levels of visual features. SinGAN [39] uses a pyramid of generators and discriminators to learn the multi-scale patch distribution in a single image. Considering the domain-specific knowledge of pan-sharpening, we design two discriminators to train against one generator for spectral and spatial preservation.

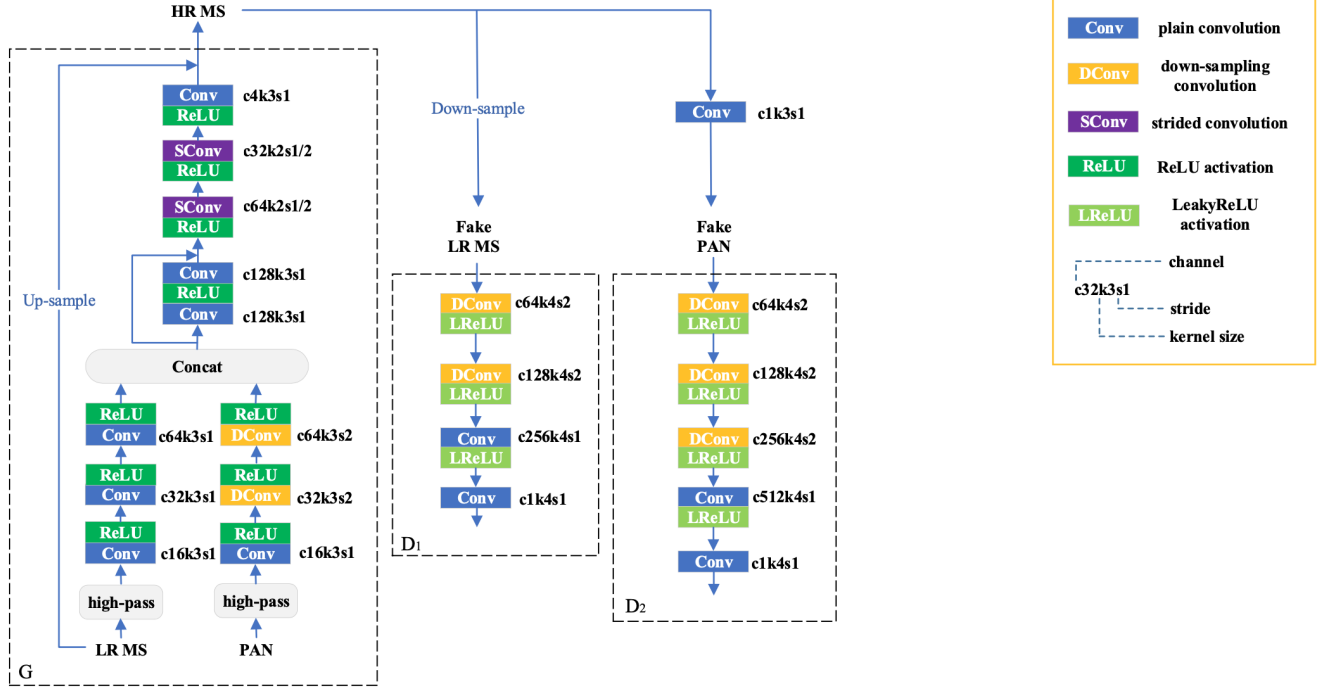


Fig. 1. The architecture of our proposed model, PGMAN. The generator takes the original LR MS and PAN images as inputs and generates the HR MS image. The pan-sharpened result will be degraded spatially and spectrally to form a pair of fake inputs for multi-adversarial learning. According to the feedback from these two discriminators, the generator will minimize the distance between the real and fake distributions and further improve the spatial and spectral quality of the fusion results. The parameters of each layer in the neural network are given on the right side.

III. METHOD

A. Network Architecture

1) *Generator Architecture*: We design the generator based on the architecture of TFNet [21] and make the following modifications to it to further improve the quality of the pan-sharpened images. Firstly, inspired by PanNet [17], the generator is trained on the high-pass domain and the output of it is added to the up-sampled LR MS image for better spectral preservation. Generally, the high-pass domain of images usually contains more spatial details. Moreover, learning the residual between the LR MS image and the final HR MS image can stabilize the training process. Secondly, considering that the input pair PAN and MS images are of different sizes, we build two independent feature extraction (FE) sub-networks. The PAN FE sub-network has two stride-2 convolutions for down-sampling, while the MS FE sub-network has two stride-1 convolutions to maintain the feature map resolution without down-sampling. We concatenate feature maps produced by these two sub-networks and append a residual block [18] to achieve fusion. Finally, two successive fractionally-strided convolutions that both are with a stride of $\frac{1}{2}$ are applied to up-sample the feature maps to meet the size of the desired HR MS. The outputs are high-frequency parts of the pan-sharpened MS images. We add them to the up-sampled LR MS images to obtain the final results. Fig. 1 shows the detailed architecture of our generator.

2) *Discriminators Architecture*: We use two discriminators for verifying the consistency in pan-sharpening process.

Firstly, we down-sample the fused images to the same spatial resolution as the LR MS images and then apply the discriminator-1 D_1 to enforce them to have the same spectral information. Secondly, the discriminator-2 D_2 is applied to match the spatial structures of the fused images to that of the PAN images. Different from [40], we don't use the global average pooling or maximum pooling to obtain the spectrally degraded version of the fused HR MS. Instead, we train an auxiliary network consisting of only one 3×3 convolution layer to estimate the transformation from MS images to PAN images. The auxiliary spectral degradation network is pre-trained individually with the LR MS and the down-sampled PAN images and will be fixed when training the generator and discriminators. We use discriminators similar to the one used in [41]. Since the input LR MS and PAN are with different image sizes and channels, the two discriminators have distinct architectures as shown in Fig. 1. D_2 has one more convolution layer to down-sample the feature maps because the PAN image has a larger image size. As suggested by WGAN-GP [35], we remove the last activation function and batch normalization layers in our discriminators.

As can be seen, our generator and discriminators are fully convolutional, which makes our model easy to train and can accept PAN and MS images with arbitrary sizes in the testing phase.

B. Loss Function

For simplification and convenience, Table I lists some key notations used in the following of this paper.

TABLE I
LIST OF NOTATIONS USED IN THIS PAPER.

Notation	Description
P	the pan-sharpened image from the generator
X	the input multi-spectral image
Y	the input panchromatic image
K	the number of bands of a MS image
P_i	the i -th band of the image P
\tilde{P}	a spatially degraded version of the image P
\hat{P}	a spectrally degraded version of the image P
N	the number of a batch
n	the id of a sample
α, β, λ	hyperparameters
GP	the gradient penalty for discriminators

1) *Q-Loss*: Supervised learning-based methods usually employ L_1 or L_2 loss to train the networks. However, under the unsupervised setting, there are no ideal images to be compared with. In this work, we attempt to devise an alternative solution that can quantify the quality of the fusion result with reference to the inputs rather than the ground truth. The intuition behind this is that there must be some consistencies across modalities, which means there is a measure that we can obtain in LR MS and PAN images and it still holds when applying it to the HR pan-sharpened MS images. Image quality index (QI) [42] provides a statistical similarity measurement between two monochrome images. To measure the spectral consistency, we can calculate the QI values between any couple of spectral bands in the LR MS image and compare them with those in the pan-sharpened image. Analogously, the QI values between each spectral band in the MS image and the PAN image should be consistent with the QI values between each spectral band in the pan-sharpened image and the PAN image, which defines the spatial consistency. The rationale behind it is, when the spectral information is translated from the coarse-scale to the fine-scale in spatial resolution, the QI values should be unchanged after fusion.

Recall that, in the pan-sharpening paradigm, the inter-relationships measured by QI between any couple of spectral bands of MS images should be unchanged after fusion, otherwise the pan-sharpened MS images may have spectral distortions. Furthermore, the inter-relationships between each band of the MS and the same sized PAN image should be preserved across scales. Therefore, the spatial and spectral consistencies can be directly calculated from the pan-sharpened image, the LR MS image, and the PAN image without the ground truth. The underlying assumption of inter-relationships consistency of cross-similarity is demonstrated by the fact that the true high-resolution MS data, whenever available, exhibit spectral and spatial distortions that are both zero, within the approximations of the model, and definitely lower than those attained by any fusion method. To describe this, quantitatively, we introduce a non-GT loss on top of QNR [26], which defined as follows:

$$\mathcal{L}_Q = 1 - QNR \quad (1)$$

QNR is the abbreviation of *Quality with No Reference*, which is a combination of D_λ and D_s . D_λ is a spectral distortion index while D_s is a spatial quality metric complementary to D_λ .

$$QNR = (1 - D_\lambda)(1 - D_s) \quad (2)$$

The optimal value of QNR is 1.

$$D_\lambda = \sqrt{\frac{2}{K(K-1)} \sum_{i=1}^K \sum_{\substack{j=1 \\ i \neq j}}^K |Q(P_i, P_j) - Q(X_i, X_j)|} \quad (3)$$

where P is the pan-sharpened result, X stands for the LR MS input and K is the number of bands. P_i and X_i represent the i th band of them, respectively. Q stands for Image quality index (QI) [42]. It is defined as follows:

$$Q(x, y) = \frac{4\sigma_{xy} \cdot \bar{x} \cdot \bar{y}}{(\sigma_x^2 + \sigma_y^2)(\bar{x}^2 + \bar{y}^2)} \quad (4)$$

where σ_{xy} means the covariance between x and y , and σ_x^2 and σ_y^2 are the variances of x and y , respectively. \bar{x} and \bar{y} are the means of x and y , respectively.

$$D_s = \sqrt{\frac{1}{K} \sum_{i=1}^K |Q(P_i, Y) - Q(X_i, \tilde{Y})|} \quad (5)$$

where Y is the panchromatic input and \tilde{Y} is the degraded low-resolution version of it.

This loss function enables us to measure the qualities of the fused images from input PAN and MS images without ground truth HR MS images.

2) *Adversarial Loss*: We design two discriminators, D_1 for spectral preservation and D_2 for spatial preservation. The generator learns to preserve more spectral information to cheat D_1 which is able to distinguish the real and fake LR MS images and preserve more spatial details to cheat D_2 which is able to distinguish the real PAN image and the spectral degraded fusion result. The loss function of the generator G takes the form of:

$$\mathcal{L}_G = \frac{1}{N} \sum_{n=1}^N -\alpha D_1(\tilde{P}^{(n)}) - \beta D_2(\hat{P}^{(n)}) + \mathcal{L}_Q(P^{(n)}, X^{(n)}, Y^{(n)}) \quad (6)$$

where N is the number of samples. P, X, Y are pan-sharpened MS, LR MS, and PAN images, respectively. \tilde{P} and \hat{P} stand for the spatially and spectrally degraded P . α and β are hyperparameters.

To stabilize the training, we employ WGAN-GP [35] as a basic framework, *i.e.*, using Wasserstein distance [34] and applying gradient penalty [35] to discriminators. The loss functions of D_1 and D_2 are formulated as follows:

TABLE II
DETAILS OF THE DATASETS USED IN OUR EXPERIMENTS

Sensor	MS bands	bit depth	#Images	Resolution (PAN/MS)	Training	Testing
GaoFen-2	4	10	7	Reduced(3.2/12.8 m)	#Patches: 24000 input PAN size: $256 \times 256 \times 1$ input LRMS size: $64 \times 64 \times 4$ output size: $256 \times 256 \times 4$	#Patches: 286 input PAN size: $400 \times 400 \times 1$ input LRMS size: $100 \times 100 \times 4$ output size: $400 \times 400 \times 4$
				Full (0.8/3.2 m)	#Patches: 24000 input PAN size: $256 \times 256 \times 1$ input LRMS size: $64 \times 64 \times 4$ output size: $256 \times 256 \times 4$	#Patches: 286 input PAN size: $400 \times 400 \times 1$ input LRMS size: $100 \times 100 \times 4$ output size: $400 \times 400 \times 4$
QuickBird	4	11	5	Reduced (2.4/9.6 m)	#Patches: 16000 input PAN size: $256 \times 256 \times 1$ input LRMS size: $64 \times 64 \times 4$ output size: $256 \times 256 \times 4$	#Patches: 40 input PAN size: $400 \times 400 \times 1$ input LRMS size: $100 \times 100 \times 4$ output size: $400 \times 400 \times 4$
				Full (0.6/2.4 m)	#Patches: 16000 input PAN size: $256 \times 256 \times 1$ input LRMS size: $64 \times 64 \times 4$ output size: $256 \times 256 \times 4$	#Patches: 828 input PAN size: $400 \times 400 \times 1$ input LRMS size: $100 \times 100 \times 4$ output size: $400 \times 400 \times 4$
WorldView-3	8	11	3	Reduced (1.6/6.4 m)	#Patches: 10000 input PAN size: $256 \times 256 \times 1$ input LRMS size: $64 \times 64 \times 4$ output size: $256 \times 256 \times 4$	#Patches: 99 input PAN size: $400 \times 400 \times 1$ input LRMS size: $100 \times 100 \times 4$ output size: $400 \times 400 \times 4$
				Full (0.4/1.6 m)	#Patches: 10000 input PAN size: $256 \times 256 \times 1$ input LRMS size: $64 \times 64 \times 4$ output size: $256 \times 256 \times 4$	#Patches: 1960 input PAN size: $400 \times 400 \times 1$ input LRMS size: $100 \times 100 \times 4$ output size: $400 \times 400 \times 4$

$$\mathcal{L}_{D_1} = \frac{1}{N} \sum_{n=1}^N -D_1(X^{(n)}) + D_1(\tilde{P}^{(n)}) + \lambda GP(D_1, X^{(n)}, \tilde{P}^{(n)}) \quad (7)$$

$$\mathcal{L}_{D_2} = \frac{1}{N} \sum_{n=1}^N -D_2(Y^{(n)}) + D_2(\hat{P}^{(n)}) + \lambda GP(D_2, Y^{(n)}, \hat{P}^{(n)}) \quad (8)$$

where GP is the gradient penalty for discriminators and λ is a hyper-parameter.

C. Training Details

Our method is implemented in PyTorch [43] and trained on a single NVIDIA Titan 1080Ti GPU. The batch size and learning rate are set as 8 and $1e-4$, respectively. The hyper-parameters in Eqs. 6, 7 and 8 are set as $\alpha = 2e - 4$, $\beta = 1e - 4$, and $\lambda = 100$. Adam optimizer [44] is used to train the model for 20 epochs with fixed hyper-parameters $\beta_1 = 0$ and $\beta_2 = 0.9$. It should be noted that, we process the images at the raw bit depth in both training and testing phases without normalizing them into displayable 8-bit images.

IV. EXPERIMENTS AND RESULTS

A. Datasets

We conduct extensive experiments on three datasets with images collected from GaoFen-2, QuickBird and WorldView-3 satellites. The detailed information of the datasets can be seen in Table II. For comparison between the supervised and unsupervised methods, we build the datasets under both reduced-scale (based on Wald's protocol [45]) and full-scale

settings. Wald's protocol has been widely used for assessment of pan-sharpening methods, in which the original MS and PAN images are spatially degraded before feeding into models, the reducing factor being the ratio between their spatial resolutions, and the original MS images are considered as reference images for comparison. Same as the previous works [40], [46], we implement it by blurring the full-resolution datasets using a Gaussian filter and then downsampling them with a scaling factor of 4. Under Wald's protocol, the supervised models can be trained on reduced-resolution images using the original MS images as labels. However, under full-resolution setting, there are no reference images so that only unsupervised models can be trained with the full-resolution images as inputs. Although the training environment is limited related to the type of models, testing is without constraints. We can test all models on both reduced-scale and full-scale images whether they need supervised labels or not.

Moreover, because of the very large size of remote sensing images, for example, PAN and MS images of GaoFen-2 are with the size of about $30,000 \times 30,000$ and $7,500 \times 7,500$ pixels, respectively, which is too large to feed into a neural network, we crop these images into small patches to form training and testing sets. As for the testing set, we crop the remote sensing images orderly in small overlapping regions between neighborhood patches to remove border effects as is the common practice. It is noted that there is no overlapping between the training and testing sets.

B. Metrics

In order to examine the performance of models on both reduced-scale and full-scale images, we use reference and non-reference metrics, respectively.

TABLE III

QUANTITY RESULTS ON GAOFEN-2 DATASET. THE BEST RESULT IN EACH GROUP IS IN **BOLD** FONT. THE LAST ROW INDICATES THE IDEAL VALUE OF EACH METRIC.

Type	Model	Non-reference Metrics			Reference Metrics		
		D_λ	D_s	QNR	SAM	ERGAS	SSIM
Traditional	BDS [9]	0.0283±0.0184	0.0451±0.0214	0.9282±0.0370	3.0869±0.3199	6.2093±0.6545	0.6969±0.0266
	GS [5]	0.0297±0.0246	0.0475±0.0316	0.9249±0.0513	1.9673±0.2051	3.7190±0.3750	0.8383±0.0181
	IHS [2]	0.0281±0.0224	0.0451±0.0316	0.9287±0.0497	2.1299±0.2151	3.8587±0.4022	0.8377±0.0183
	Brovey [47]	0.0246±0.0168	0.0505±0.0302	0.9265±0.0418	1.7377±0.2054	3.4325±0.3198	0.8293±0.0172
	HPF [48]	0.0204±0.0116	0.0182±0.0079	0.9618±0.0175	2.0829±0.2312	4.1046±0.4477	0.8097±0.0199
	LMM [49]	0.0221±0.0138	0.0250±0.0139	0.9537±0.0256	1.8137±0.2233	6.3369±0.6827	0.6397±0.0274
	SFIM [8]	0.0178±0.0113	0.0193±0.0074	0.9634±0.0166	1.9509±0.1881	4.2613±0.4855	0.8085±0.0212
Supervised	PNN [15]	0.0147±0.0106	0.0313±0.0144	0.9544±0.0149	1.2717±0.1157	1.4982±0.1995	0.9626±0.0064
	DRPNN [19]	0.0168±0.0087	0.0695±0.0294	0.9150±0.0308	1.2162±0.1203	1.2838±0.1509	0.9708±0.0041
	MSDCNN [20]	0.0131±0.0076	0.0409±0.0229	0.9465±0.0232	1.4422±0.1543	1.4904±0.2065	0.9629±0.0064
	PanNet [17]	0.0113±0.0072	0.1234±0.0429	0.8669±0.0458	1.0881±0.1140	1.2923±0.1655	0.9712±0.0046
	PSGAN [23]	0.0082±0.0042	0.1012±0.0360	0.8914±0.0373	1.0572±0.1040	1.2092±0.1427	0.9745±0.0038
Unsupervised	Pan-GAN [40]	0.0347±0.0188	0.0274±0.0179	0.9392±0.0342	2.6423±0.2697	5.2453±0.5608	0.7318±0.0242
	PGMAN	0.0077±0.0043	0.0134±0.0107	0.9790±0.0129	2.0100±0.1947	2.6394±0.2978	0.9166±0.0111
Ideal Value		0	0	1	0	0	1

TABLE IV

QUANTITY RESULTS ON QUICKBIRD DATASET. THE BEST RESULT IN EACH GROUP IS IN **BOLD** FONT. THE LAST ROW INDICATES THE IDEAL VALUE OF EACH METRIC.

Type	Model	Non-reference Metrics			Reference Metrics		
		D_λ	D_s	QNR	SAM	ERGAS	SSIM
Traditional	BDS [9]	0.0110±0.0000	0.0202±0.0003	0.9690±0.0004	2.0508±0.1499	3.7505±0.5481	0.7940±0.0028
	GS [5]	0.0202±0.0003	0.0433±0.0011	0.9377±0.0018	1.5325±0.0631	2.7242±0.3269	0.8684±0.0019
	IHS [2]	0.0222±0.0002	0.0476±0.0012	0.9315±0.0017	1.8226±0.0624	2.8254±0.3321	0.8605±0.0019
	Brovey [47]	0.0226±0.0002	0.0435±0.0010	0.9353±0.0018	1.5730±0.0291	2.7190±0.2970	0.8600±0.0019
	HPF [48]	0.0094±0.0000	0.0429±0.0007	0.9481±0.0008	1.7227±0.0668	3.1126±0.2483	0.8489±0.0011
	LMM [49]	0.0105±0.0000	0.0389±0.0006	0.9510±0.0006	1.6070±0.0320	2.9798±0.2548	0.8367±0.0015
	SFIM [8]	0.0088±0.0000	0.0441±0.0008	0.9476±0.0008	1.5982±0.0460	3.1296±0.2503	0.8496±0.0011
Supervised	PNN [15]	0.0467±0.0004	0.0927±0.0004	0.8652±0.0011	2.5468±0.0887	3.3448±0.1668	0.9020±0.0005
	DRPNN [19]	0.0182±0.0001	0.0500±0.0003	0.9329±0.0006	2.1292±0.0765	2.2699±0.1625	0.9235±0.0005
	MSDCNN [20]	0.0654±0.0004	0.1116±0.0009	0.8307±0.0018	3.1420±0.0617	3.2128±0.1386	0.8897±0.0008
	PanNet [17]	0.0048±0.0000	0.0409±0.0002	0.9545±0.0003	1.4493±0.0683	1.7392±0.1650	0.9465±0.0003
	PSGAN [23]	0.0297±0.0001	0.0668±0.0005	0.9055±0.0007	2.1482±0.0530	2.1682±0.0808	0.9266±0.0002
Unsupervised	Pan-GAN [40]	0.0082±0.0046	0.0286±0.0177	0.9633±0.0173	2.6317±0.3126	2.2248±0.2379	0.9192±0.0125
	PGMAN	0.0037±0.0024	0.0202±0.0087	0.9762±0.0093	1.7902±0.1838	2.2581±0.3308	0.9076±0.0182
Ideal Value		0	0	1	0	0	1

1) *Non-reference Metrics*: On full-resolution, there is no ground truth and we use the non-reference metrics, which can be calculated without the target. D_λ , D_s and QNR are widely used non-reference metrics in pan-sharpening task, which have been introduced in Section III to support our loss function.

2) *Reference Metrics*: Under Wald's protocol [45], we can also validate models on reduced-resolution where the PAN and MS images are down-sampled so that the origin MS image is as ground truth. Therefore on low-resolution, we use the reference metrics:

- **SAM** [50] measures spectral distortions of pan-sharpened images comparing with the reference images.

$$SAM(x_1, x_2) = \arccos\left(\frac{x_1 \cdot x_2}{\|x_1\| \cdot \|x_2\|}\right) \quad (9)$$

where x_1 , x_2 are two spectral vectors from the pan-sharpened result and the reference result.

- **ERGAS** [51] The *erreur relative globale adimensionnelle de synthèse* (ERGAS), also known as the relative global

dimensional synthesis error is a commonly used global quality index. It is given by:

$$ERGAS = 100 \frac{h}{l} \sqrt{\frac{1}{N} \sum_{i=1}^N \left(\frac{RMSE(B_i)}{M(B_i)} \right)^2} \quad (10)$$

where h and l are the spatial resolutions of PAN and MS images; $RMSE(B_i)$ is the root mean square error between the i th band of the fused and reference image; $M(B_i)$ is the mean value of the original MS band B_i .

- **SSIM** [52] is a widely used metric which models the loss and distortion according to the similarities in light, contrast, and structure information.

$$SSIM(x, y) = \frac{(2\mu_x\mu_y + c_1)(2\sigma_{xy} + c_2)}{(\mu_x^2 + \mu_y^2 + c_1)(\sigma_x^2 + \sigma_y^2 + c_2)} \quad (11)$$

where σ_{xy} means the covariance between x and y , and σ_x^2 and σ_y^2 are the variances of x and y , respectively. μ_x

TABLE V

QUANTITY RESULTS ON WOLDVIEW-3 DATASET. THE BEST RESULT IN EACH GROUP IS IN **BOLD** FONT. THE LAST ROW INDICATES THE IDEAL VALUE OF EACH METRIC.

Type	Model	Non-reference Metrics			Reference Metrics		
		D_λ	D_s	QNR	SAM	ERGAS	SSIM
Traditional	BSD [9]	0.0260±0.0321	0.0733±0.0641	0.9044±0.0835	5.4941±0.9020	5.5417±0.6988	0.8493±0.0274
	GS [5]	0.0461±0.0525	0.1087±0.0796	0.8542±0.1150	5.9630±0.5248	6.2308±0.6185	0.8309±0.0246
	IHS [2]	0.0574±0.0642	0.1121±0.0849	0.8421±0.1273	6.2706±0.7805	6.3862±0.6681	0.8199±0.0269
	Brovey [47]	0.0429±0.0418	0.1042±0.0708	0.8601±0.0979	5.6566±0.9382	6.2390±0.6842	0.8338±0.0254
	HPF [48]	0.0386±0.0396	0.0804±0.0574	0.8862±0.0840	5.5389±0.8940	6.7569±1.0258	0.8102±0.0356
	LMM [49]	0.0433±0.0446	0.0759±0.0575	0.8865±0.0879	5.7981±0.9798	6.9729±1.1321	0.8084±0.0364
	SFIM [8]	0.0384±0.0437	0.0754±0.0512	0.8909±0.0803	5.3298±0.8431	7.3518±1.9554	0.8154±0.0361
Supervised	PNN [15]	0.0412±0.0402	0.0445±0.0340	0.9171±0.0633	5.2637±0.5915	4.1083±0.5081	0.9250±0.0191
	DRPNN [19]	0.0478±0.0352	0.0533±0.0250	0.9020±0.0492	6.1427±0.5190	4.5375±0.3573	0.9301±0.0145
	MSDCNN [20]	0.0415±0.0424	0.0494±0.0321	0.9122±0.0635	5.2105±0.5746	4.2856±0.5286	0.9225±0.0187
	PanNet [17]	0.0374±0.0410	0.0355±0.0327	0.9294±0.0639	4.8066±0.5473	4.3263±0.5742	0.9180±0.0202
	PSGAN [23]	0.0392±0.0456	0.0534±0.0335	0.9108±0.0674	4.5523±0.5049	4.1070±0.4402	0.9311±0.0192
Unsupervised	Pan-GAN [40]	0.0396±0.0449	0.0638±0.0529	0.9013±0.0839	5.9902±1.0484	7.1762±1.2440	0.7857±0.0434
	PGMAN	0.0129±0.0128	0.0409±0.0242	0.9469±0.0327	6.3959±0.9904	6.8348±1.2325	0.7617±0.0563
Ideal Value		0	0	1	0	0	1

and μ_y are the means of x and y , respectively. c_1 and c_2 are fixed constants.

C. Comparison with State-of-the-arts

Fourteen methods including seven traditional methods, five supervised methods, and two unsupervised methods are employed for comparison:

Traditional methods include BSD [9], GS [5], IHS [2], Brovey [47], HPF [48], LMM [49] and SFIM [8].

Supervised methods are PNN [15], DRPNN [19], MSD-CNN [20], PanNet [17] and PSGAN [23]. These methods are state-of-the-art supervised deep learning based pan-sharpening methods. The first four models are CNN-based models and the last one is based on GAN.

Unsupervised methods include Pan-GAN [40] and our proposed PGMAN.

D. Quantitative Results

For non-reference metrics, D_λ is used to examine the spectral distortions in full-scale images, D_s is for the spatial distortions, and QNR is a comprehensive metric. For reference metrics, SAM is used to examine the spectral distortions in reduced-scale images, ERGAS is for the spatial distortions, and SSIM is a comprehensive metric.

Table III shows the quantitative assessments on GaoFen-2. The best value in each group is in **bold** font. For the non-reference metrics, our proposed PGMAN takes the advantage of the unsupervised learning and obtains the best average values on D_λ , D_s and QNR, which is much better than all the other competitors. As for the reference metrics, unsupervised methods fall behind supervised methods because they do not utilize the label information while the supervised methods can directly minimize the difference between the output pan-sharpened images and the ground truth. Nevertheless, our proposed PGMAN still obtains the best results among the unsupervised methods on the reference metrics. PGMAN also

achieves better values than all of the traditional methods in terms of ERGAS and SSIM.

Table IV shows the quantitative assessments on QuickBird. Similar to the results of GaoFen-2 dataset, here, our proposed model, PGMAN maintains its superiority and achieves the best values on all non-reference metrics, which exceed the performance of other traditional and supervised methods. PGMAN also obtains the best value in terms of SAM in the unsupervised methods, while is a little behind Pan-GAN on ERGAS and SSIM.

And we also conduct an evaluation on the 8-band images from WorldView-3 dataset. Table V shows the quantitative assessments on it. The results show that our proposed PGMAN still maintains its superiority and achieves the best values on all non-reference metrics, showing the effectiveness and the great practical value of it. For the reference metrics, both unsupervised methods fall a lot. In 8-band WV3 dataset, the generalization ability from the full-scale dataset to the reduced-scale dataset may be affected due to the added spectral bands. It remains a challenge to the unsupervised methods trained in the full-scale dataset.

Generally, traditional models do not rely on any training data and make a medium performance regardless of the kind of testing environment. Supervised methods tend to be better on the reduced-scale images because they make full use of the supervision information and directly minimize the loss between the predicted pan-sharpened and the ground truth images. However, this may make them overfit the reduced-scale images and generalize poorly on full-resolution test images, and sometimes these methods even perform worse than traditional models. The best non-reference metrics achieved by supervised methods are PNN (GaoFen-2 dataset, Table III) and PanNet (QuickBird dataset, Table IV), the reason may be that they consist of fewer parameters (see Table VIII) and thus with lower possibility to become overfitting. Here, unsupervised models take the advantages of learning from the full-scale images and obtain the best non-reference metrics. Furthermore, our proposed model, PGMAN, surpasses all

TABLE VI

ABLATION STUDY OF THE LOSS FUNCTION ON GAOFEN-2 DATASET. “√” MEANS INCLUDING THE REFERRED LOSS ITEM. THE LAST ROW INDICATES THE IDEAL VALUE OF EACH METRIC.

Loss item		Non-reference Metrics			Reference Metrics		
\mathcal{L}_Q	\mathcal{L}_{adv}	D_λ	D_s	QNR	SAM	ERGAS	SSIM
✓	✓	0.0072±0.0036	0.1117±0.0369	0.8819±0.0377	2.3673±0.2382	3.4380±0.4005	0.8375±0.0228
✓		0.0080±0.0061	0.0182±0.0119	0.9740±0.0162	2.1384±0.1838	2.8171±0.3070	0.9074±0.0108
✓	✓	0.0077±0.0043	0.0134±0.0107	0.9790±0.0129	2.0100±0.1947	2.6394±0.2978	0.9166±0.0111
Ideal Value		0	0	1	0	0	1

TABLE VII

PARAMETER ANALYSIS ON GAOFEN-2 DATASET.

Parameter		Non-reference Metrics			Reference Metrics		
α	β	D_λ	D_s	QNR	SAM	ERGAS	SSIM
1e-3	2e-3	0.0080±0.0045	0.0136±0.0085	0.9786±0.0107	2.1021±0.1727	2.7228±0.2840	0.9112±0.0111
2e-3	1e-3	0.0074±0.0040	0.0222±0.0088	0.9706±0.0094	1.9444±0.1955	2.4874±0.2799	0.9130±0.0112
1e-4	2e-4	0.0087±0.0036	0.0144±0.0102	0.9770±0.0112	2.0712±0.1856	2.7020±0.2962	0.9135±0.0114
2e-4	1e-4	0.0077±0.0043	0.0134±0.0107	0.9790±0.0129	2.0100±0.1947	2.6394±0.2978	0.9166±0.0111
1e-5	2e-5	0.0074±0.0039	0.0139±0.0098	0.9788±0.0115	2.2276±0.1949	2.9133±0.3134	0.9080±0.0115
0	0	0.0080±0.0061	0.0182±0.0119	0.9740±0.0162	2.1384±0.1838	2.8171±0.3070	0.9074±0.0108
Ideal Value		0	0	1	0	0	1

other unsupervised methods. Our method significantly improves the results, which indicates that full-resolution images indeed provide rich spatial and spectral information and are helpful for improving the quality of the pan-sharpened images. Although our method falls behind the supervised methods when testing on the reduced-scale images, considering that there is no ground truth used in our method, the results are quite promising. And more importantly, the proposed PGMAN obtains the best QNR when applied to full-resolution images, showing the great practical value of it.

E. Visual Results

Fig. 2 shows some example results on GaoFen-2 full-resolution images, which are produced from the original PAN and LR MS images. The results of Brovey (Fig. 2(f)), LMM (Fig. 2(h)) cannot preserve the spectral information from the LR MS image (Fig. 2(b)) very well. They tend to produce notable color distortions. Those supervised methods including PNN (Fig. 2(j)), DRPNN (Fig. 2(k)), MSDCNN (Fig. 2(l)), PanNet (Fig. 2(m)) and PSGAN (Fig. 2(n)) also demonstrate low quality spatial scenario details. It seems that the knowledge learned from the reduced-scale images is hard to generalize well to the real scenarios. This is because different from natural images, remote sensing images usually contain deeper bit depth and are with different pixel distribution. Down-sampling the original PAN and LR MS images in a supervised manner will change the data distribution and hurt the original information. However, when trained on the full-scale images, the quality is improved significantly for PGMAN (Fig. 2(p)). This gives us strong motivations to propose an unsupervised model since the pan-sharpening works are usually done on the full-resolution images in real applications.

Fig. 3 shows some example results on QuickBird full-resolution images. GS (Fig. 3(d)), IHS (Fig. 3(e)) and Brovey (Fig. 3(f)) distort the spectral information from the LR MS

image (Fig. 3(b)) which can be seen from the color of the roof. The supervised methods including PNN (Fig. 3(j)) and MSDCNN (Fig. 3(l)) also produce unsatisfactory results with some distortions. Our method generates the pan-sharpened image (Fig. 3(p)) with good spatial and spectral quality. The visual results from these two datasets demonstrate the superiority of our proposed model and show the advantage of unsupervised models for training on the original data distribution.

F. Ablation Study

We conduct ablation studies on GaoFen-2 dataset to verify the effectiveness of the proposed Q-loss. The quantitative results are listed in Table VI.

It is observed that using only the adversarial loss to optimize the network degrades the performance except for D_λ index. Adversarial loss tries to simulate the generation of PAN and MS images, *i.e.*, the PAN and MS images are degradation version of the desired HR MS image along the spatial and spectral dimension, respectively. However, since the inverse of the process is ill-posed, even if the degraded images of the generated pan-sharpened images are identical to the corresponding PAN and LR MS, it is hard to guarantee that the pan-sharpened images are high fidelity in both spatial and spectral information. Q-loss makes an additional constraint to the learning, *i.e.*, the spatial and spectral information should be preserved across scales. Experimental results show that Q-loss produces better results than adversarial loss in most cases, indicating that Q-loss is a stronger constraint than adversarial loss. And finally, combining the two losses together further improves the performance, especially on the reference-based indicators. Therefore, with the help of Q-loss item and adversarial loss item, our proposed model PGMAN can be optimized to a good status and achieve competitive results on both reduced-scale and full-scale images.

TABLE VIII

INFERENCE TIME AND NUMBER OF TRAINABLE PARAMETERS. NOTE THAT THE PAN-SHARPENED IMAGES ARE WITH A SIZE OF $400 \times 400 \times 4$, WE GIVE AVERAGE TIME ON THEM. AS FOR THE GAN-BASED MODELS, WE ONLY TAKE THE PARAMETERS OF THE GENERATOR INTO ACCOUNT.

Processor	Method	Time(s)	#Params
Intel Core i7-7700HQ CPU@2.80GHz	BDSO [9]	1.2613	-
	GS [5]	0.1205	-
	IHS [2]	0.0121	-
	Brovey [47]	0.0125	-
	HPF [48]	0.1061	-
	LMM [49]	0.1062	-
	SFIM [8]	0.1063	-
NVIDIA GeForce RTX 2080Ti	PNN [15]	0.0001	$\sim 0.080M$
	DRPNN [19]	0.0186	$\sim 1.639M$
	MSDCNN [20]	0.0014	$\sim 0.262M$
	PanNet [17]	0.0004	$\sim 0.077M$
	PSGAN [23]	0.0008	$\sim 1.654M$
	Pan-GAN [40]	0.0002	$\sim 0.092M$
	PGMAN (ours)	0.0004	$\sim 0.385M$

Furthermore, we also conduct parameter analysis on GaoFen-2 Dataset, where we try 6 different combinations of α and β values. Table VII displays the results. At the same magnitude, the results of $\alpha = 2\beta$ are better than those of $\beta = 2\alpha$. It indicates that giving more weights to D_1 to make a balance is good for our model to learn, because the parameters of D_1 is less than D_2 . When the magnitude is changed from $1e - 3$ to 0, we can find that both too small and too large values can affect the performance of the model. Considering all reference metrics and non-reference metrics, we finally choose $\alpha = 2e - 4$ and $\beta = 1e - 4$ to construct the loss function.

G. Efficiency Study

We evaluate the computational time and memory cost of ours and the comparison methods. All traditional methods are implemented using Matlab and run on an Intel Core i7-7700HQ CPU, and deep models are implemented in PyTorch and tested on a single NVIDIA GeForce RTX 2080Ti GPU. Table VIII shows the inference speed and number of parameters of all comparative models. The inference speed is evaluated on 286 test samples, and each pair consists of a PAN image with $400 \times 400 \times 1$ pixels and a LR MS image with $100 \times 100 \times 4$ pixels. The time is calculated by averaging these 286 samples. Additionally, we report the number of trainable parameters of all deep learning related methods.

BDSO is the slowest method, whose inference time is about 1.2613 seconds per image. IHS and Brovey only require about 0.01 seconds which are the fastest in traditional methods.

Beneficial from the advance of GPU architectures, the inference time of deep learning models is satisfactory, almost all deep models only require less than 0.001 seconds to pan-sharpen one image, except for DRPNN model who is the largest deep model with deeper network architecture and much bigger convolution filters. PNN is the fastest since it consists of only three convolution layers. PGMAN is efficient in both model size and inference speed.

V. CONCLUSION

In this paper, we propose a novel unsupervised generative multi-adversarial model for pan-sharpening, called PGMAN. PGMAN consists of one generator and two discriminators to reduce both the spectral and spatial distortions. To further improve the performance, we also introduce a QNR related loss to the unsupervised manner. As one of the advantages of unsupervised methods, our proposed method can be trained on either reduced-scale or full-scale images without ground truth. Our model is focused on original PAN and LR MS images without any preprocessing step to keep the consistency with the real application environment. The attractive performance on full-scale testing and satisfactory results on reduced-scale images demonstrate the powerful ability of our proposed model.

However, there is still a gap between the supervised and unsupervised models on the reference metrics. When we use the GAN-based framework for spectral preservation, we simply down-sample the output to form a fake LR MS image for the discriminator to recognize. The method of down-sampling remains uncertain and may affect the performance of the model, which is also an ill-posed problem. There may be another better way to achieve the degradation process to discuss. In our future work, we will continue to study the architecture of unsupervised pan-sharpening models and further improve the performance.

REFERENCES

- [1] Y. Zhang, "Understanding image fusion," *Photogramm. Eng. Remote Sens.*, vol. 70, no. 6, pp. 657–661, 2004.
- [2] T.-M. Tu, P. S. Huang, C.-L. Hung, and C.-P. Chang, "A fast intensity-hue-saturation fusion technique with spectral adjustment for ikonos imagery," *IEEE Geoscience and Remote Sensing Letters*, vol. 1, no. 4, pp. 309–312, 2004.
- [3] P. Kwarteng and A. Chavez, "Extracting spectral contrast in landsat thematic mapper image data using selective principal component analysis," *Photogramm. Eng. Remote Sens.*, vol. 55, no. 1, pp. 339–348, 1989.
- [4] V. K. Shettigara, "A generalized component substitution technique for spatial enhancement of multispectral images using a higher resolution data set," *Photogrammetric Engineering and Remote Sensing*, vol. 58, no. 5, pp. 561–567, 1992.
- [5] C. A. Laben and B. V. Brower, "Process for enhancing the spatial resolution of multispectral imagery using pan-sharpening," Jan. 4 2000, uS Patent 6,011,875.
- [6] B. Aiazzi, L. Alparone, S. Baronti, A. Garzelli, and M. Selva, "Mtf-tailored multiscale fusion of high-resolution ms and pan imagery," *Photogrammetric Engineering & Remote Sensing*, vol. 72, no. 5, pp. 591–596, 2006.
- [7] F. Palsson, J. R. Sveinsson, M. O. Ulfarsson, and J. A. Benediktsson, "Mtf-based deblurring using a wiener filter for cs and mra pansharpening methods," *IEEE Journal of Selected Topics in Applied Earth Observations and Remote Sensing*, vol. 9, no. 6, pp. 2255–2269, 2016.
- [8] J. Liu, "Smoothing filter-based intensity modulation: A spectral preserve image fusion technique for improving spatial details," *International Journal of Remote Sensing*, vol. 21, no. 18, pp. 3461–3472, 2000.
- [9] A. Garzelli, F. Nencini, and L. Capobianco, "Optimal mmse pan sharpening of very high resolution multispectral images," *IEEE Transactions on Geoscience and Remote Sensing*, vol. 46, no. 1, pp. 228–236, 2007.
- [10] J. Johnson, A. Alahi, and L. Fei-Fei, "Perceptual losses for real-time style transfer and super-resolution," in *European conference on computer vision*. Springer, 2016, pp. 694–711.
- [11] J. Cai, Z. Meng, and C. M. Ho, "Residual channel attention generative adversarial network for image super-resolution and noise reduction," in *Proceedings of the IEEE/CVF Conference on Computer Vision and Pattern Recognition Workshops*, 2020, pp. 454–455.

- [12] D. Ulyanov, A. Vedaldi, and V. Lempitsky, "Instance normalization: The missing ingredient for fast stylization," *arXiv preprint arXiv:1607.08022*, 2016.
- [13] S. Maeda, "Unpaired image super-resolution using pseudo-supervision," in *Proceedings of the IEEE/CVF Conference on Computer Vision and Pattern Recognition*, 2020, pp. 291–300.
- [14] L. Wang, D. Li, Y. Zhu, L. Tian, and Y. Shan, "Dual super-resolution learning for semantic segmentation," in *Proceedings of the IEEE/CVF Conference on Computer Vision and Pattern Recognition*, 2020, pp. 3774–3783.
- [15] G. Masi, D. Cozzolino, L. Verdoliva, and G. Scarpa, "Pansharpening by convolutional neural networks," *Remote Sensing*, vol. 8, no. 7, p. 594, 2016.
- [16] C. Dong, C. C. Loy, K. He, and X. Tang, "Image super-resolution using deep convolutional networks," *IEEE transactions on pattern analysis and machine intelligence*, vol. 38, no. 2, pp. 295–307, 2015.
- [17] J. Yang, X. Fu, Y. Hu, Y. Huang, X. Ding, and J. Paisley, "Pannet: A deep network architecture for pan-sharpening," in *Proceedings of the IEEE international conference on computer vision*, 2017, pp. 5449–5457.
- [18] K. He, X. Zhang, S. Ren, and J. Sun, "Deep residual learning for image recognition," in *Proceedings of the IEEE conference on computer vision and pattern recognition*, 2016, pp. 770–778.
- [19] Y. Wei, Q. Yuan, H. Shen, and L. Zhang, "Boosting the accuracy of multispectral image pansharpening by learning a deep residual network," *IEEE Geoscience and Remote Sensing Letters*, vol. 14, no. 10, pp. 1795–1799, 2017.
- [20] Q. Yuan, Y. Wei, X. Meng, H. Shen, and L. Zhang, "A multiscale and multidepth convolutional neural network for remote sensing imagery pan-sharpening," *IEEE Journal of Selected Topics in Applied Earth Observations and Remote Sensing*, vol. 11, no. 3, pp. 978–989, 2018.
- [21] X. Liu, Q. Liu, and Y. Wang, "Remote sensing image fusion based on two-stream fusion network," *Information Fusion*, vol. 55, pp. 1–15, 2020.
- [22] O. Ronneberger, P. Fischer, and T. Brox, "U-net: Convolutional networks for biomedical image segmentation," in *International Conference on Medical image computing and computer-assisted intervention*. Springer, 2015, pp. 234–241.
- [23] Q. Liu, H. Zhou, Q. Xu, X. Liu, and Y. Wang, "Psgan: A generative adversarial network for remote sensing image pan-sharpening," *IEEE Transactions on Geoscience and Remote Sensing*, 2020.
- [24] I. J. Goodfellow, J. Pouget-Abadie, M. Mirza, B. Xu, D. Warde-Farley, S. Ozair, A. Courville, and Y. Bengio, "Generative adversarial networks," *arXiv preprint arXiv:1406.2661*, 2014.
- [25] J.-Y. Zhu, T. Park, P. Isola, and A. A. Efros, "Unpaired image-to-image translation using cycle-consistent adversarial networks," in *Proceedings of the IEEE international conference on computer vision*, 2017, pp. 2223–2232.
- [26] L. Alparone, B. Aiazzi, S. Baronti, A. Garzelli, F. Nencini, and M. Selva, "Multispectral and panchromatic data fusion assessment without reference," *Photogrammetric Engineering & Remote Sensing*, vol. 74, no. 2, pp. 193–200, 2008.
- [27] J. Zhong, B. Yang, G. Huang, F. Zhong, and Z. Chen, "Remote sensing image fusion with convolutional neural network," *Sensing and Imaging*, vol. 17, no. 1, p. 10, 2016.
- [28] C. Szegedy, W. Liu, Y. Jia, P. Sermanet, S. Reed, D. Anguelov, D. Erhan, V. Vanhoucke, and A. Rabinovich, "Going deeper with convolutions," in *Proceedings of the IEEE conference on computer vision and pattern recognition*, 2015, pp. 1–9.
- [29] K. Simonyan and A. Zisserman, "Very deep convolutional networks for large-scale image recognition," *arXiv preprint arXiv:1409.1556*, 2014.
- [30] Y. Rao, L. He, and J. Zhu, "A residual convolutional neural network for pan-sharpening," in *2017 International Workshop on Remote Sensing with Intelligent Processing (RSIP)*. IEEE, 2017, pp. 1–4.
- [31] Y. Wei, Q. Yuan, H. Shen, and L. Zhang, "Boosting the accuracy of multispectral image pansharpening by learning a deep residual network," *IEEE Geoscience and Remote Sensing Letters*, vol. 14, no. 10, pp. 1795–1799, 2017.
- [32] A. Radford, L. Metz, and S. Chintala, "Unsupervised representation learning with deep convolutional generative adversarial networks," *arXiv preprint arXiv:1511.06434*, 2015.
- [33] X. Mao, Q. Li, H. Xie, R. Y. Lau, Z. Wang, and S. Paul Smolley, "Least squares generative adversarial networks," in *Proceedings of the IEEE international conference on computer vision*, 2017, pp. 2794–2802.
- [34] M. Arjovsky, S. Chintala, and L. Bottou, "Wasserstein generative adversarial networks," in *International conference on machine learning*. PMLR, 2017, pp. 214–223.
- [35] I. Gulrajani, F. Ahmed, M. Arjovsky, V. Dumoulin, and A. Courville, "Improved training of wasserstein gans," *arXiv preprint arXiv:1704.00028*, 2017.
- [36] H. Zhang, I. Goodfellow, D. Metaxas, and A. Odena, "Self-attention generative adversarial networks," in *International conference on machine learning*. PMLR, 2019, pp. 7354–7363.
- [37] I. Durugkar, I. Gemp, and S. Mahadevan, "Generative multi-adversarial networks," *arXiv preprint arXiv:1611.01673*, 2016.
- [38] W. Tang, G. Li, X. Bao, F. Nian, and T. Li, "Mscgan: Multi-scale conditional generative adversarial networks for person image generation," in *2020 Chinese Control And Decision Conference (CCDC)*. IEEE, 2020, pp. 1440–1445.
- [39] T. R. Shaham, T. Dekel, and T. Michaeli, "Singan: Learning a generative model from a single natural image," in *Proceedings of the IEEE/CVF International Conference on Computer Vision*, 2019, pp. 4570–4580.
- [40] J. Ma, W. Yu, C. Chen, P. Liang, X. Guo, and J. Jiang, "Pan-gan: An unsupervised pan-sharpening method for remote sensing image fusion," *Information Fusion*, vol. 62, pp. 110–120, 2020.
- [41] P. Isola, J.-Y. Zhu, T. Zhou, and A. A. Efros, "Image-to-image translation with conditional adversarial networks," in *Proceedings of the IEEE conference on computer vision and pattern recognition*, 2017, pp. 1125–1134.
- [42] Z. Wang and A. C. Bovik, "A universal image quality index," *IEEE signal processing letters*, vol. 9, no. 3, pp. 81–84, 2002.
- [43] A. Paszke, S. Gross, F. Massa, A. Lerer, J. Bradbury, G. Chanan, T. Killeen, Z. Lin, N. Gimelshein, L. Antiga et al., "Pytorch: An imperative style, high-performance deep learning library," *arXiv preprint arXiv:1912.01703*, 2019.
- [44] D. P. Kingma and J. Ba, "Adam: A method for stochastic optimization," *arXiv preprint arXiv:1412.6980*, 2014.
- [45] L. Wald, T. Ranchin, and M. Mangolini, "Fusion of satellite images of different spatial resolutions: Assessing the quality of resulting images," *Photogrammetric engineering and remote sensing*, vol. 63, no. 6, pp. 691–699, 1997.
- [46] S. Luo, S. Zhou, Y. Feng, and J. Xie, "Pansharpening via unsupervised convolutional neural networks," *IEEE Journal of Selected Topics in Applied Earth Observations and Remote Sensing*, vol. 13, pp. 4295–4310, 2020.
- [47] A. R. Gillespie, A. B. Kahle, and R. E. Walker, "Color enhancement of highly correlated images. ii. channel ratio and "chromaticity" transformation techniques," *Remote Sensing of Environment*, vol. 22, no. 3, pp. 343–365, 1987.
- [48] U. G. Gangkofner, P. S. Pradhan, and D. W. Holcomb, "Optimizing the high-pass filter addition technique for image fusion," *Photogrammetric Engineering & Remote Sensing*, vol. 73, no. 9, pp. 1107–1118, 2007.
- [49] S. de Béthune, F. Muller, and J.-P. Donnay, "Fusion of multispectral and panchromatic images by local mean and variance matching filtering techniques," *Fusion of Earth Data*, pp. 28–30, 1998.
- [50] R. H. Yuhas, A. F. Goetz, and J. W. Boardman, "Discrimination among semi-arid landscape endmembers using the spectral angle mapper (sam) algorithm," in *Proc. Summaries 3rd Annu. JPL Airborne Geosci. Workshop*, vol. 1, 1992, pp. 147–149.
- [51] L. Wald, "Quality of high resolution synthesised images: Is there a simple criterion?" in *Third conference" Fusion of Earth data: merging point measurements, raster maps and remotely sensed images"*. SEE/URISCA, 2000, pp. 99–103.
- [52] Z. Wang, A. C. Bovik, H. R. Sheikh, and E. P. Simoncelli, "Image quality assessment: from error visibility to structural similarity," *IEEE transactions on image processing*, vol. 13, no. 4, pp. 600–612, 2004.

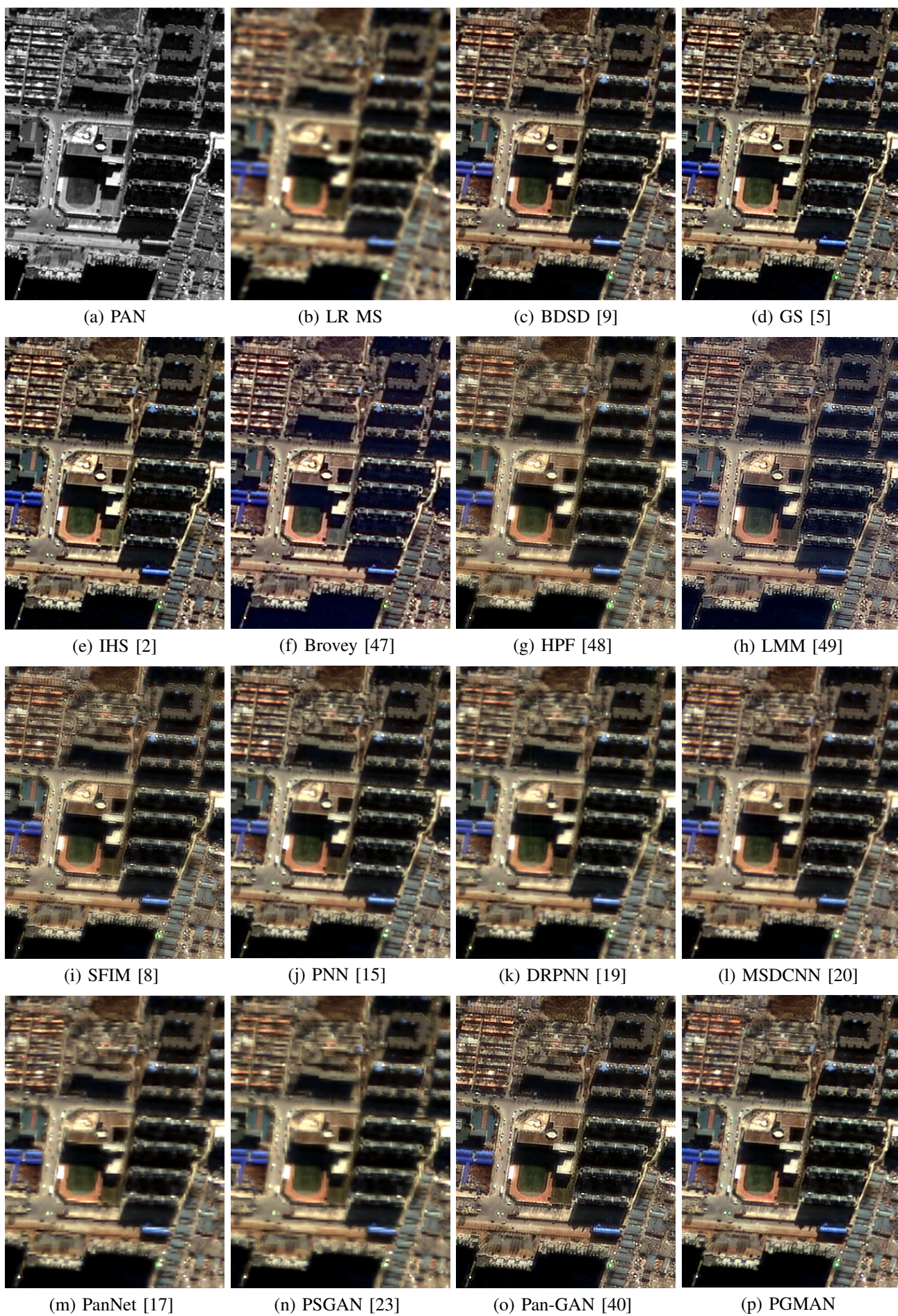


Fig. 2. Visual results on GaoFen-2 full-resolution dataset.

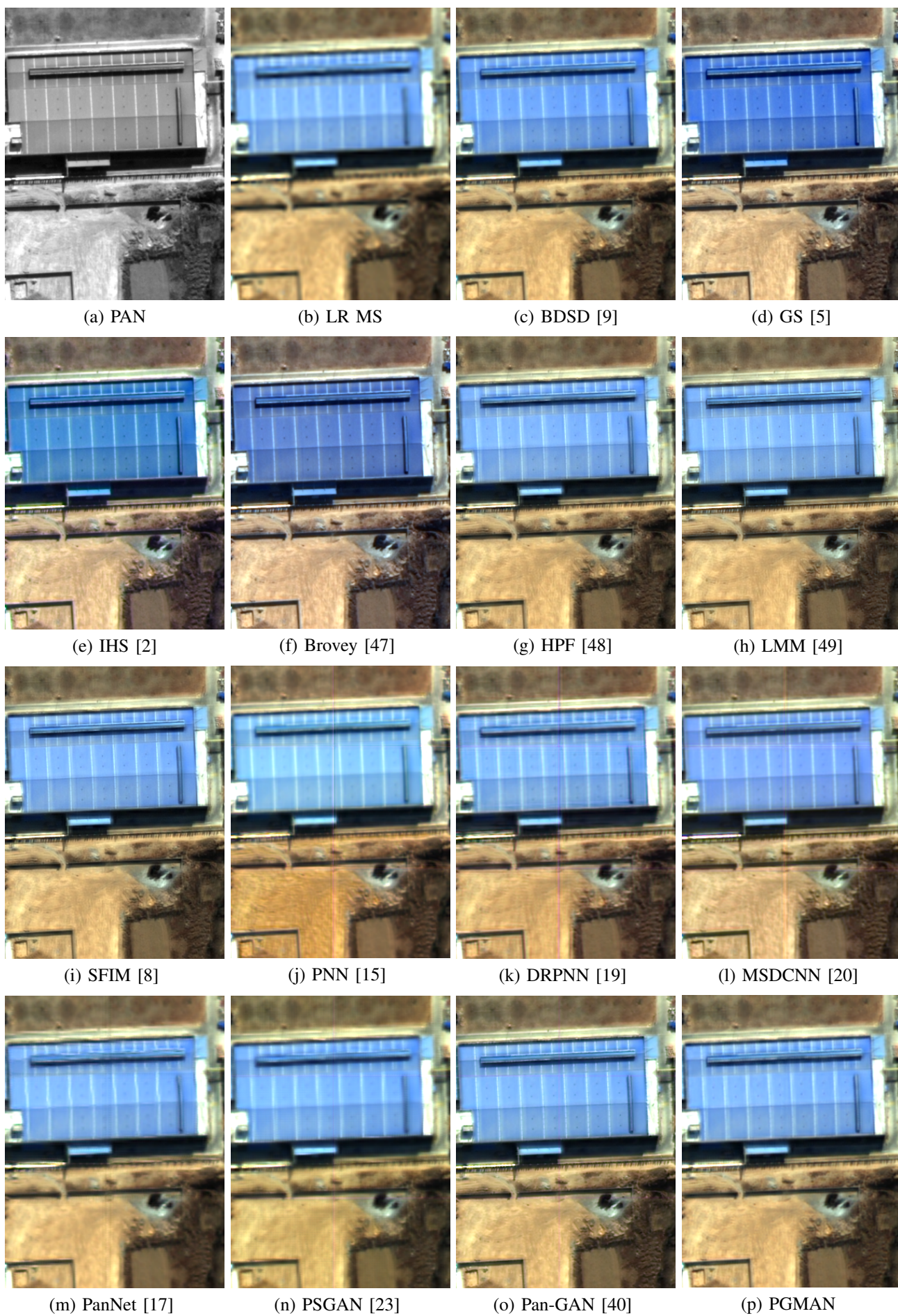


Fig. 3. Visual results on QuickBird full-resolution dataset.